ISBN: 978-3-95450-179-3 doi:10.18429/JACoW-FEL2017-MOP053



# HIGH SPECTRAL DENSITY COMPTON BACK-SCATTERED GAMMA-RAY SOURCES AT FERMILAB *

D. Mihalcea[1], B. Jacobson[2], A. Khizhanok[3], A. Murokh[2], P. Piot[1,4], and J. Ruan[4]
[1] Department of Physics and Northern Illinois Center for Accelerator & Detector Development, Northern Illinois University, DeKalb, USA
[2] Radiabeam Technologies, Santa Monica, USA
[3] Department of Mechanical Engineering, Northern Illinois University, DeKalb, USA
[4] Fermi National Accelerator Laboratory, Batavia, USA

*Abstract*

A ~ 1.2 MeV gamma-ray source is planned to be built at Fermilab following the completion of the ~ 300 MeV superconducting linac. The high energy photons are back-scattered from the interactions between electrons and high intensity IR laser pulses. In this contribution we discuss some of the experiment design challenges and evaluate the performances of the *gamma*-ray source. We expect the peak brilliance to be of the order of $10^{23}$ photons/[s-(mm mrad)$^2$ 0.1% BW] and the spectral density of the radiation in excess of $2 \times 10^5$ photons/s/eV.

## INTRODUCTION

Gamma-ray sources are extensively used in various fields from biomedical and fundamental research applications to industry and national defense. The required performances of the $\gamma$-ray sources are dictated by the application, but for most cases, large values of peak brightness, photon flux, and a small energy bandwidth are desired. Typically, high precision experiments would require high brightness sources and others, like biomedical and industrial applications, would mostly benefit from higher beam fluxes.

Gamma-ray sources consisting of back-scattered radiation resulting during the collisions of energetic electrons and laser pulses [1], process also known as Inverse Compton Scattering (ICS), became attractive due to the progress in producing high quality GeV-class electron beams and very high intensity lasers. The size and the cost of these $\gamma$-sources are mostly driven by the electron beam accelerator. Recent progress in the field of laser plasma wakefield accelerators (LPWA) [2] made possible building compact $\gamma$-ray sources with very high brightness [3, 4] but with relatively low photon flux due to the low operating frequency ( 10 Hz). To overcome this problem our approach is to use the superconducting 300 MeV Fermilab injector to be built at FAST facility, which can deliver up to 15,000 electron pulses per second.

In this paper we present the design of the proposed $\gamma$-ray source and the expected performances based on simulations.

* This work was sponsored by the DNDO award 2015-DN-077-ARI094 to Northern Illinois University. Fermilab is operated by Fermi Research Alliance, LLC. for the U.S. Department of Energy under contract DE-AC02-07CH11359.

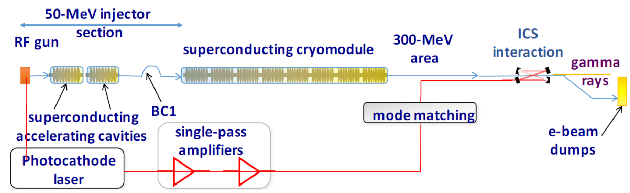


Figure 1: Linac layout at FAST facility.

## ICS EXPERIMENT SETUP

The most relevant components of the FAST linac are shown in Fig. 1. The electrons are extracted by photoemission from a $CsTe_2$ cathode illuminated with picosecond long UV laser pulses. The acceleration is performed by a normal conducting RF gun, two superconducting TESLA cavities and a superconducting cryomodule consisting of eight TESLA cavities. The operating RF frequency is 1.3 GHz the final electron energy is up to 300 MeV and the charge of each electron pulse is up to 5 nC. More details about the linac and beam dynamics simulations can be found in Refs. [5, 6]. The low energy section of the linac, consisting of the gun and the two booster cavities, was successfully tested in the summer of 2016 and the full completion, testing and some experiments are expected to take place in the summer of 2017.

The laser system, already functional, can produce up 10 $\mu$J IR pulses at 3 MHz sampling rate. The IR laser pulses are split in two components: the first component contains about 10% of the total energy and it is sent to the photocathode via two stages of frequency doubling crystals. The second component is further amplified to about 0.5 mJ/pulse and sent to the ICS experimental area. Up to five equally spaced RF macropulses are generated each second. The duration of each macropulse is 1 ms and and trains of about 3,000 electron bunches can be emitted during this time.

The LINAC components most relevant for this experiment are those used for the final focus of the electron beam. Thirty centimeters upstream of the interaction point (IP) there are three permanent magnetic quadrupoles (PMQs) (Fig. 2) manufactured by Radiabeam. They are hollow cylinders with outer radius 15 mm, inner radius 4 mm and lengths 3 cm, 6 cm, and 3 cm respectively. The spacing between them is 5 cm. The lens strengths of the PMQs in the preliminary design are -150 m$^{-1}$, 150 m$^{-1}$ and -150 m$^{-1}$. Symmetrically, there are three more identical PMQs downstream of

ISBN: 978-3-95450-179-3 doi:10.18429/JACoW-FEL2017-MOP053

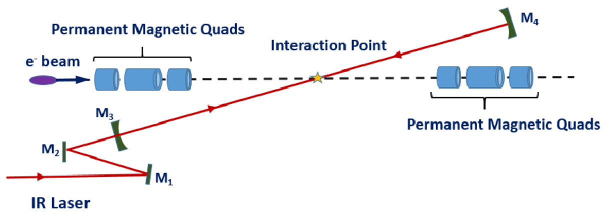


Figure 2: Simplified view of the interaction region. PMQs are symmetrically located 30 cm upstream and downstream of the interaction point (IP). Fabry-Perot (FB) high finesse enhancement cavity consists of the concave mirrors $M_3$ and $M_4$. The angle between electron beam direction of propagation and FB axis is about $5^0$. Optical elements for laser beam matching, feed-back components and the additional Herriott cell are not shown.

the IP. The final focus region also includes four adjustable quadrupoles located upstream of the first set of PMQs. These quadrupoles allow matching the beam into the PMQs such that certain requirements on the beam at IP are met.

Before its arrival at the interaction region, the IR laser beam travels through a delay stage to ensure the synchronization with the electron beam at IP. The delay stage is driven by the electrical signal provided by a photoconductive THz antenna inserted into the beamline [7].

The IR beam is directed to a Fabry-Perot (FB) resonator, see Fig. 2, where beam intensity is amplified by a factor of at least 10 due to coherent addition of the laser pulse which bounces inside the cavity and the incoming pulses produced by the laser system [8]. To match the eigenfrequencies of the $\approx$ 1 m long resonator with the 3 MHz laser sampling rate, the FB cavity is coupled to a Herriott cell [9] which extends the total propagation distance inside the resonator. With this addition we estimate that the amplification factor is at least 50.

## FINAL FOCUS OPTIMIZATION

The electron beam quality is critical to the overall performance of the $\gamma$-ray source. Electron beam transverse emittance ($\epsilon_\perp$), transverse spot size at IP ($\sigma_e$), bunch duration ($\tau_e$), charge ($e\dot{N}_e$), energy ($W = \gamma m_e c^2$), beam divergence ($\sigma_e'$), and repetition rate in addition to laser pulse energy (proportional with IR photon number $N_l$) and laser beam waist ($w_0$) completely determine the most important parameters of the scattered radiation [10, 11]: brightness ($B_x$), photon flux ($N_x$) and $\gamma$-ray bandwidth (BW).

$$B_x \propto \frac{N_l}{w_0^2}\gamma^2\frac{N_e}{\tau_e \epsilon_\perp^2} \tag{1}$$

$$N_x \approx \frac{N_e N_l \sigma_T}{2\pi\left(\sigma_e^2 + \frac{w_0^2}{4}\right)} \tag{2}$$

$$BW \equiv \frac{\delta\omega_x}{\omega_x} \approx 2\gamma^2\sigma_e'^2 \tag{3}$$

where $\sigma_T$ in Eqn. 2 is the total Thompson cross section and $\omega_x$ in Eqn. 3 is the scattered radiation frequency.

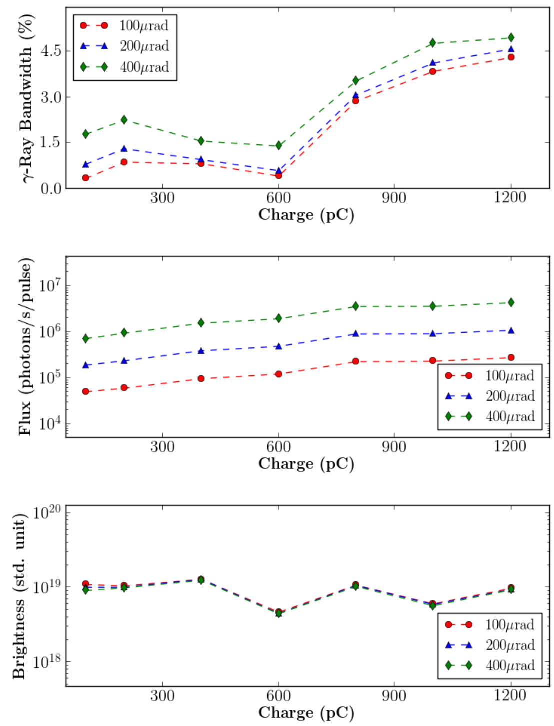


Figure 3: Scattered radiation bandwidth, flux and brightness as functions of electron beam charge and for three values of collimator opening angle.

The validity condition for Eqn. 2 requires that the transverse size of the two beams at IP are about the same. In this experiment the scattered photon flux is mostly constrained by the laser beam waist which in our design is $w_0 = 30$ $\mu$m. The expression of the scattered radiation bandwidth in Eqn. 3 is valid when electron beam transverse emittance is the dominant contributor to the $\gamma$-ray energy spread. The contributions from electron beam energy spread (< 0.1 %) and laser bandwidth (< 0.2 %) are negligible in comparison with at least 0.5 % we expect from electron beam emittance. Energy spread due to the opening angle of the collimator that captures the scattered radiation should also be considered. Equation 3 shows that electrons with angular spread of about 100 $\mu$rad (rms) and beam energy close to 250 MeV generate scattered radiation with energy spread of 0.5 % provided only beam emittance is considered.

To maximize the scattered photon flux the electron beam spot size at IP should be close to the laser beam waist. Also, to minimize the $\gamma$-ray bandwidth, the angular spread of the electrons should be at a minimum. Since the transverse emittance does not change much in the final focus region and spot size at IP is constrained ($\sigma_e = \frac{w_0}{2}$), electrons angular spread minimization can be achieved by reducing the correlation between the transverse position and the divergence that is the electron beam Twiss parameter $\alpha_e \approx 0$. The two conditions are:

$$\sigma_e = \frac{w_0}{2}, \qquad \text{and} \qquad \alpha_e = 0. \tag{4}$$

ISBN: 978-3-95450-179-3 doi:10.18429/JACoW-FEL2017-MOP053



Figure 3 shows brightness, bandwidth, and photon flux as functions of electron beam charge and the three values of the collimator opening angle: 100 $\mu$rad, 200 $\mu$rad, and 400 $\mu$rad. Larger electron beam charge leads to larger transverse emittance, higher bandwidth and higher photon flux. The weak dependence of bandwidth with opening angle shows that electron beam emittance has by far the largest contribution to the scattered radiation energy spread increase. Table 1 summarizes the scattered radiation parameters, evaluated with the code described in [10], and Table 2 contains the relevant parameters of the electron beam and IR laser.

Table 1: $\gamma$-ray Parameters for Different Collimator Opening Angles Generated by the Collision Between a Single Electron Bunch of Charge 100 pC and Energy 259 MeV and an IR Laser Pulse. The Last Column Corresponds to the Whole Scattered Radiation.

| Opening angle | 100 $\mu$rad | 200 $\mu$rad | > 10 mrad |
|---|---|---|---|
| Brightness (std. units) | $1.1 \times 10^{19}$ | $1.0 \times 10^{19}$ | $1.1 \times 10^{18}$ |
| Flux (photons) | $5.0 \times 10^{4}$ | $1.9 \times 10^{5}$ | $1.4 \times 10^{7}$ |
| Bandwidth (%) | 0.34 | 0.80 | 49.8 |

Table 2: Electron Beam and Laser Main Parameters.

| Electron beam | | Laser pulse | |
|---|---|---|---|
| Beam energy (MeV) | 259.0 | wavelength (nm) | 1053 |
| Beam charge (pC) | 100 | pulse energy (J) | 0.5 |
| Energy spread (%) | 0.06 | bandwidth (%) | 0.2 |
| Duration (ps) | 5.0 | Duration (ps) | 3.0 |
| Beam size x/y ($\mu$m) | 12/13 | waist ($\mu$m) | 30 |
| Emittance ($\mu$m) | 0.34 | | |

As suggested in Ref. [12], an important figure of merit of the $\gamma$-ray source is spectral density defined as $\delta \equiv \frac{N_{ph}}{\delta E \delta t}$. Assuming scattered radiation bandwidth lower than 1 % the spectral density we can achieve from a single electron bunch collision is $\delta \approx 19.8$ photons/s/eV, when beam charge is 100 pC and opening angle 200 $\mu$rad. Since about 15,000 electron bunches can be generated each second we expect the spectral density to be above $2 \times 10^5$ /photons/s/eV. Higher spectral density can be obtained by increasing the collimator opening angle and electron bunch charge. In this case the photon dose becomes significantly larger at the expense of slightly higher bandwidth (Fig. 3).

The conditions on electron beam at IP stated in Eqn. 4 can only approximately be fulfilled with the four adjustable quadrupoles in the final focus region. The "tails" of the electron beam angular distributions at IP, see Fig. 4, increase the scattered radiation bandwidth. One way (not tested yet) to decrease the electron beam divergence at IP is to also use some of the quadrupoles located upstream of the final focus region.

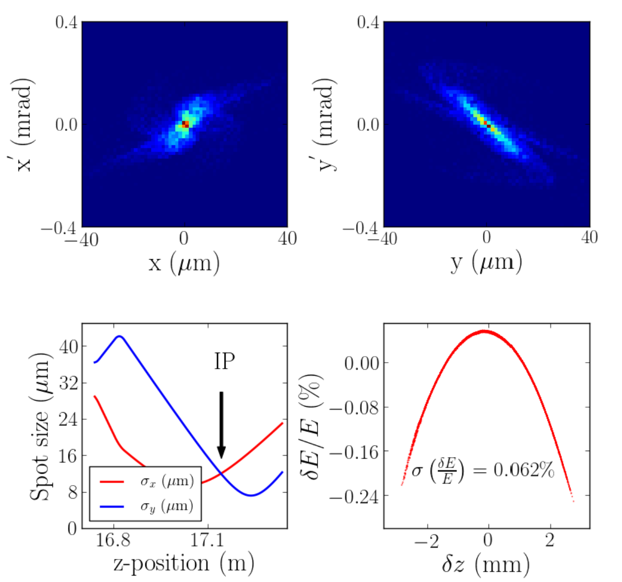


Figure 4: Top: x-x′ and y-y′ distributions at IP for a 100 pC electron beam. Bottom: $\sigma_x$ and $\sigma_y$ values upstream of IP (left) and longitudinal electron beam energy spread (right).

## CONCLUSIONS

Beam simulations from cathode to IP were performed to determine the realistic electron bunch distribution just prior to the collision with the IR laser pulse. The final focus region contains four medium strength adjustable quadrupoles and six small ultra-high strength permanent magnetic quadrupoles. The laser pulse energy is enhanced with a Fabry-Perot optical cavity coupled to a Herriott cell to match resonator eigenfrequencies with laser sampling rate.

The electron beam transverse size is matched with the laser beam waist at IP, $\sigma_e = \frac{w_0}{2} \approx 15$ $\mu$m and electrons divergence is minimized by setting the Twiss parameter $\alpha \approx 0$. The scattered radiation brightness is of the order of $10^{19}$ photons/[s-(mm-mrad)$^2$-BW(0.1%)] and photon flux $1.9 \times 10^5$ photons/s from a single 100 pC electron bunch and collimator opening angle of 200 $\mu$rad. The $\gamma$-ray photons have energy of 1.2 MeV bandwidth of 0.8 % and spectral density 19.8 photons/s/eV from a single bunch. Photon flux, brightness and spectral density are enhanced by a factor of 15,000 representing the electron beam repetition rate.

## REFERENCES

[1] O. Kulikov, Y. Telnov and M. Yakimenko, *Phys. Lett.*, **13**, 344, 1964.

[2] E. Esarey, C. B. Schroeder, and W. P. Leemans, Physics of laser-driven plasma-based accelerators, *Rev. Mod. Phys.*, **81**, 12291285, 2009.

[3] K. Ta Phuoc, S. Corde, C. Thaury, V. Malka, A. Tafzi, J. P. Goddet, R. C. Shah, S. Sebban, and A. Rousse, All-optical

ISBN: 978-3-95450-179-3 doi:10.18429/JACoW-FEL2017-MOP053

Compton gamma-ray source, *Nat. Photonics*, **6**, 308311, 2012.

[4] S. Chen, *et al.*, MeV-energy X rays from Inverse Compton Scattering with laser-wakefield accelerated electrons, *Phys. Rev. Lett.* **110**, 155003, 2013.

[5] J. Leibfritz *et al.*, in *Proceedings of the PAC11*, New York, USA, 2011.

[6] P. Piot, Y.-E. Sun, and M. Church, in *Proceedings of the IPAC10*, Kyoto, Japan, 2010.

[7] B. Jacobson, Fermilab IOTA Workshop, June 15, 2016.

[8] H. Shimizu, A. Aryshev, Y. Higashi, Y. Honda, and J. Urakawa, *NIMA*, **745**, 63-72, 2014.

[9] D. R. Herriott, H. Kogelnik, and R. Kompfner, *Appl. Opt.*, **3**, 523, 1964.

[10] W. J. Brown and F. V. Hartemann, *Phys. Rev. ST Accel. Beams*, **7**, 060703, 2004.

[11] W. J. Brown and F. V. Hartemann, *AIP Conference Proceedings*, **737**, 839, 2004.

[12] A. Bacci, *et al.*, *J. of Applied Physics*, **113**, 194508, 2013.